SUPPLEMENTARY MATERIAL OF "NEURAL ODES FOR MAGNETIC HOLOGRAPHIC QCD PHASE DIAGRAM"

This supplementary material provides a detailed discussions we have made in the main text. We give the equations of motion for the hairy black holes and show all thermodynamic quantities. We then introduce the calculation method and neural ODEs.

Equations of motion and thermodynamics

By varying the action, the field equations can be obtained:

$$\begin{aligned}
\nabla_\mu\nabla^\mu\phi-\frac{\partial_\phi Z}{4}F_{\mu\nu}F^{\mu\nu}-\frac{\partial_\phi\hat{Z}}{4}\hat{F}_{\mu\nu}\hat{F}^{\mu\nu}-\partial_\phi V=0\\
\nabla^\nu(ZF_{\nu\mu})=0\\
\nabla^\nu(\hat{Z}\hat{F}_{\nu\mu})=0\\
R_{\mu\nu}-\frac{1}{2}Rg_{\mu\nu}=\frac{1}{2}\nabla_\mu\phi\nabla_\nu\phi+\frac{Z}{2}F_{\mu\rho}F^\rho_\nu+\frac{\hat{Z}}{2}\hat{F}_{\mu\rho}\hat{F}^\rho_\nu+\frac{1}{2}\left(-\frac{1}{2}\nabla_\mu\phi\nabla^\mu\phi-\frac{Z}{4}F_{\mu\nu}F^{\mu\nu}-\frac{\hat{Z}}{4}\hat{F}_{\mu\nu}\hat{F}^{\mu\nu}-V\right)g_{\mu\nu}\,.
\end{aligned}\tag{S1}$$

The bulk black hole solutions are

$$\begin{aligned}
ds^2=-f(r)e^{-\eta(r)}dt^2+\frac{dr^2}{f(r)}+r^2(dx^2+dy^2+g(r)dz^2)\,,\\
\phi=\phi(r),\quad A=A(r)dt,\quad \hat{A}=\frac{B}{2}(xdy-ydx)\,,
\end{aligned}\tag{S2}$$

where r is the holographic radial coordinate with the AdS boundary located at $r\to\infty$. The blackening function $f(r)$ is vanishing at the event horizon $r=r_h$ at which the temperature and entropy density are given by

$$T=\frac{1}{4\pi}f'(r_h)e^{-\eta(r_h)/2},\quad s=\frac{2\pi}{\kappa_N^2}r_h^3\,.\tag{S3}$$

Note that the magnetic field in the z-direction breaks isotropy.

Substituting the ansatz (S2) into (S1) gives six equations:

$$\begin{aligned}
\phi''(r)+\left(\frac{f'(r)}{f(r)}+\frac{1}{2}\left(\frac{6}{r}+\frac{g'(r)}{g(r)}-\eta'(r)\right)\right)\phi'(r)-\frac{V'(\phi}{f(r)}+\frac{e^{\eta(r)}A'(r)^2Z'(\phi(r))}{2f(r)}-\frac{B^2\hat{Z}'(\phi)}{2r^4f(r)}=0\,,\\
A''(r)+\frac{1}{2}A'(r)\left(\frac{6}{r}+\frac{g'(r)}{g(r)}+\eta'(r)+\frac{2Z'(\phi)\phi'(r)}{Z(\phi)}\right)=0\,,\\
\eta'(r)+\frac{-r^3(f(r)+rf'(r))g'(r)+g(r)\left(B^2\hat{Z}(\phi)+r^4f(r)\phi'(r)^2\right)}{r^3f(r)\left(3g(r)+rg'(r)\right)}=0\,,\\
f'(r)+\frac{1}{2}f(r)\left(\frac{4}{r}+\frac{g'(r)}{g(r)}-\eta'(r)\right)+\frac{1}{3}rV(\phi)+\frac{B^2\hat{Z}(\phi)}{3r^3}+\frac{1}{6}e^{\eta(r)}r\hat{Z}(\phi)A'(r)^2=0\,,\\
g''(r)-\frac{g'(r)^2}{2g(r)}+g'(r)\left(\frac{2}{r}+\frac{\eta'(r)}{2}\right)+g(r)\left(\frac{3\eta'(r)}{r}+\phi'(r)^2\right)=0\,,
\end{aligned}\tag{S4}$$

where five of them are independent.

The form of $V(\phi)$ and $Z(\phi)$ is taken from [S1].

$$\begin{aligned}
V(\phi)=-12\cosh[c_1\phi]+(6c_1^2-\frac{3}{2})\phi^2+c_2\phi^6\,,\\
Z(\phi)=\frac{1}{1+c_3}\mathrm{sech}[c_4\phi^3]+\frac{c_3}{1+c_3}e^{-c_5\phi}\,.
\end{aligned}\tag{S5}$$

Expansion at the UV boundary $r \to \infty$ yields

$$\begin{aligned}
\phi(r) =& \frac{\phi_s}{r} + \frac{(\phi_v + \frac{1}{6}(-1+6c_1^4)\phi_s^3 \ln[r])}{r^3} + \frac{B^2\hat{Z}'(0)}{6r^4} + \cdots , \\
g(r) =& 1 + \frac{g_4 - \frac{1}{4}B^2 \ln[r]\hat{Z}(0)}{r^4} + \frac{B^2\phi_s\hat{Z}'(0)}{5r^5} + \cdots , \\
\eta(r) =& 1 + \frac{\phi_s^2}{6r^2} + \frac{g_4}{r^4} + \frac{\frac{1}{144}\left((1-6c_1^4)\phi_s^4 + 72\phi_s\phi_v + 12B^2\hat{Z}(0)\right)}{r^4} + \frac{1}{12}\frac{\ln[r]\left(-((1-6c_1^4)\phi_s^4) - 3B^2\hat{Z}(0)\right)}{r^4} \\
&+ \frac{16B^2\phi_s\hat{Z}'(0)}{45r^5} + \cdots , \\
A(r) =& \mu_B - \frac{2\kappa_N^2 n_B}{2r^2} + \frac{2\kappa_N^2 n_B\phi_s Z'(0)}{3r^3 Z(0)} + \frac{2\kappa_N^2 n_B\phi_s^2\left(Z(0)^2 - 12Z'(0)^2 + 6Z(0)Z''(0)\right)}{48r^4 Z(0)^2} + \cdots ,
\end{aligned} \tag{S6}$$

where we have taken the normalization of the spacetime coordinates at the boundary such that $\eta(r \to \infty) = 0$ and $g(r \to \infty) = 1$. Expansion at the event horizon $r = r_h$ gives

$$\begin{aligned}
f =& f_h(r - r_h) + \cdots , \\
\eta =& \eta_h + \eta_1(r - r_h) + \cdots , \\
A =& A_h(r - r_h) + \cdots , \\
\phi =& \phi_h + \phi_1(r - r_h) + \cdots , \\
g =& g_h + g_1(r - r_h) + \cdots .
\end{aligned} \tag{S7}$$

After substituting (S7) into the EoMs (S4), one finds five independent coefficients $(r_h, A_h, \eta_h, \phi_h, g_h)$.

The relationship between the free energy density Ω and the on-shell action S is:

$$-\Omega V = T(S + S_\partial)_{on-shell} , \tag{S8}$$

where V is the spatial volume of the boundary system. The boundary term is given by

$$S_\partial = \frac{1}{2\kappa_N^2}\int_{r\to\infty} d^4x\sqrt{-h}\left[2K - 6 - \frac{1}{2}\phi(r)^2 - \left(\frac{6c_1^4 - 1}{12}\right)\phi(r)^4 \ln[r] - b\phi(r)^4 + \frac{1}{4}(F_{\mu\nu}F^{\mu\nu} + \hat{Z}(0)\hat{F}_{\mu\nu}\hat{F}^{\mu\nu}) \ln[r]\right] . \tag{S9}$$

Here, $h_{\mu\nu}$ is the induced metric at the UV boundary with $K_{\mu\nu}$ the extrinsic curvature defined by the outward pointing normal vector to the boundary.

The boundary energy-momentum tensor reads

$$\begin{aligned}
T_{\mu\nu} =& \lim_{r\to\infty} \frac{2r^2}{\sqrt{-h}}\frac{\delta(S + S_\partial)}{\delta h^{\mu\nu}} , \\
=& \frac{1}{2\kappa_N^2}\lim_{r\to\infty} r^2\Big[2(Kh_{\mu\nu} - K_{\mu\nu} - 3h_{\mu\nu}) - (\frac{1}{2}\phi^2 + \frac{6c_1^4 - 1}{12}\phi^4 \ln[r] + b\phi^4)h_{\mu\nu} \\
&- (F_{\mu\rho}F^\rho_\nu - \frac{1}{4}h_{\mu\nu}F_{\rho\lambda}F^{\rho\lambda}) \ln[r] - \hat{Z}(0)(\hat{F}_{\mu\rho}\hat{F}^\rho_\nu - \frac{1}{4}h_{\mu\nu}\hat{F}_{\rho\lambda}\hat{F}^{\rho\lambda}) \ln[r]\Big] .
\end{aligned} \tag{S10}$$

Substituting the UV expansion on the boundary gives:

$$\epsilon = T_{tt} = \frac{(1+48b)\phi_s^4}{96\kappa_N^2} + \frac{\phi_s\phi_v}{2\kappa_N^2} + \frac{-144f_v + 192g4 + 12B^2\hat{Z}[0]}{96\kappa_N^2} , \tag{S11}$$

$$p_x = p_y = T_{xx} = T_{yy} = \frac{(3 - 48b - 8c_1^4)\phi_s^4}{96\kappa_N^2} + \frac{\phi_s\phi_v}{2\kappa_N^2} + \frac{-48f_v - 8B^2\hat{Z}[0]}{96\kappa_N^2} , \tag{S12}$$

$$-\Omega = p_z = T_{zz} = \frac{(3 - 48b - 8c_1^4)\phi_s^4}{96\kappa_N^2} + \frac{\phi_s\phi_v}{2\kappa_N^2} + \frac{-48f_v + 4(48g4 + B^2\hat{Z}[0])}{96\kappa_N^2} . \tag{S13}$$

Note that in the thermodynamic limit $V \to \infty$, $\Omega = -p_z$. From the EoMs (S4), we can get a radially conserved charge:

$$Q = e^{\frac{\eta(r)}{2}}\sqrt{g(r)}r^3\left(r^2\left(e^{-\frac{\eta(r)}{2}}\frac{f(r)}{r^2}\right)' - Z(\phi)A(r)A'(r)\right) - B^2\int_{r_h}^{r}\frac{e^{-\frac{\eta(r_s)}{2}}\sqrt{g(r_s)}\hat{Z}[\phi(r_s)]}{r_s}dr_s\,, \tag{S14}$$

which connects data from the horizon to the UV boundary. Evaluating it at both the horizon and the boundary yields

$$Q = Ts = \epsilon - \Omega - \mu_B n_B = \epsilon^{total} - \Omega - \mu_B n_B - BM\,, \tag{S15}$$

where $\epsilon^{total} = \epsilon + \epsilon^{field}$ is the total energy including the external field $\epsilon^{field} = BM$ with M the magnetization. This is the expected thermodynamic relation. More precisely, M can be computed by the partial derivative of the free energy with respect to B.

$$M = -\left(\frac{\partial\Omega}{\partial B}\right)_{T,\mu_B} = -\int_{r_h}^{\infty}\frac{B\sqrt{e^{-\eta(r)}g(r)}\hat{Z}[\phi(r)]}{r}dr + \lim_{r\to\infty}\frac{B\sqrt{e^{-\eta(r)}f(r)g(r)}\ln[r]\hat{Z}[0]}{r}\,. \tag{S16}$$

It can be checked straightforwardly that the first law of thermodynamics

$$d\Omega = -sdT - n_B d\mu_B - MdB\,, \tag{S17}$$

is satisfied. One can then obtain the magnetic susceptibility $\chi_B = \left(\frac{\partial M}{\partial B}\right)_{T,\mu_B}$.

Following [S1], we choose $c_1 = 0.7100, c_2 = 0.0037, c_3 = 1.935, c_4 = 0.085, c_5 = 30$ of (S5). Moreover, we take $\kappa_N^2 = 2\pi(1.68), \phi_s = 1085\text{MeV}$ and $b = -0.27341$.

Calculation method and neural ODEs

Neural networks and neural ODEs have been intensively utilized in holographic QCD literature (e.g. [S2–S5]). In particular, neural networks have been effectively integrated into ODE frameworks in [S3, S4]. In our approach, we introduce a novel neural ODE architecture to numerically solve the magnetic coupling $\hat{Z}[\phi(z)]$, constrained by lattice QCD data with high precision. We model $\hat{Z}$ using a feedforward neural network with three hidden layers, each structured as $x = \sigma(\text{weight} \times x' + \text{bias})$, where the activation function is $\sigma = \tanh$. Here, x and x' represent the output and input of each layer, respectively, and $H = \{\text{weight, bias}\}$ is the parameter set. The layer structure is [input(1)-(16)-(64)-(16)-output(1)]. Details for reproducibility are provided below.

Fig. S1 illustrates our computational approach. To address the inverse problem of mapping lattice QCD data to a holographic model, we initialize a trial function $\hat{Z}(\phi)$, used to solve the bulk EoMs (S4) with asymptotic AdS boundary conditions and regular horizon conditions. The solution yields boundary field theory observables, which are then compared to lattice QCD data to iteratively refine $\hat{Z}(\phi)$. Due to scaling symmetries, there are three independent IR data points: A_h, ϕ_h, and B_F, corresponding to the field values at the event horizon and a pre-scaled magnetic field. These map to the UV quantities—temperature T, chemical potential μ_B, and physical magnetic field B_T—where B_T is the transformed field after scaling. By modeling $\hat{Z}(\phi)$ through a neural network, we solve the EOMs and obtain thermodynamic quantities such as T, μ_B, B_T, M, s, χ_B, and Δp_z.

Since the lattice data [S6] covers only a small region at zero chemical potential, the values of T, μ_B, and B_T computed with an arbitrary set of A_h, ϕ_h, and B_F cannot adequately cover this region. Therefore, as shown in Fig. S1, it is necessary to adjust A_h, ϕ_h, and B_F to obtain a set that effectively covers the relevant lattice QCD region. The values of the remaining thermodynamic quantities M, S, χ_B, and Δp_z depend on the choice of the trial function $\hat{Z}(\phi)$. To optimize $\hat{Z}(\phi)$, we define a loss function $\mathrm{L} = \mathrm{L}(M, s, \chi_B, \Delta p_z)$. We can obtain the optimal $\hat{Z}(\phi)$ by iteratively applying gradient descent (Adam: α =0.0002, β_1=0.9, β_2=0.999) to minimize the loss function [S7]. Since our model's high precision requirements, we have to employ a neural network ODE model [S8] to solve for $\hat{Z}(\phi)$ throughout the entire process. This model effectively transforms the conventional neural network into a continuous form, facilitating differential equations' rapid and accurate solutions.

For later convenience, one can rephrase the EoMs (S4) as the following form:

$$\frac{d\Theta}{dz} = \Xi(z, \Theta, \dot{\Theta}(z), \hat{Z}(\Phi), \hat{Z}'(\Phi), B_F), \quad \Theta(z) = \begin{pmatrix}\Phi(z)\\ F(z)\\ \eta(z)\\ A(z)\\ g(z)\end{pmatrix}\,, \tag{S18}$$

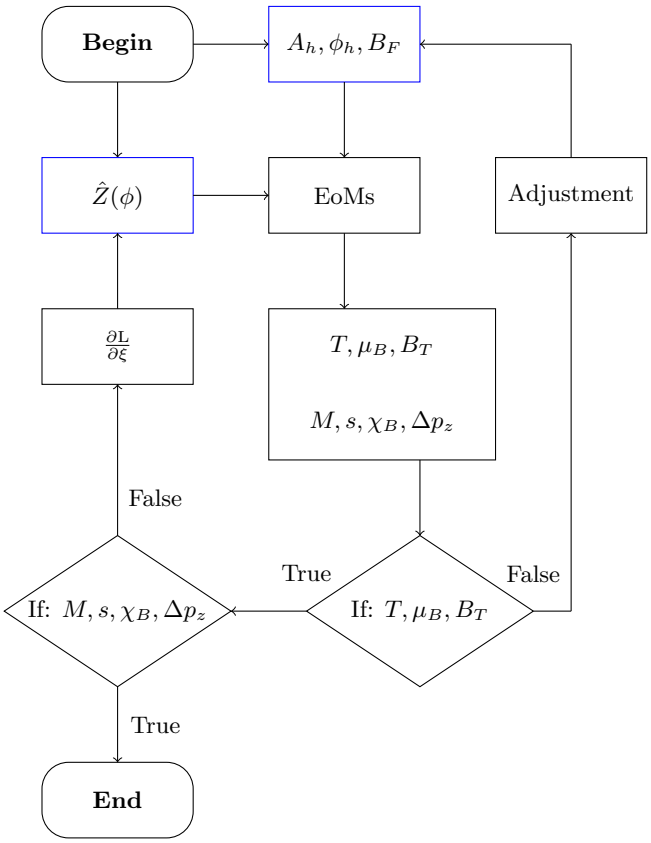

FIG. S1. Illustration of the Algorithm process: Given a trial functional $\hat{Z}(\phi)$ and a set of (A_h, ϕ_h, B_F). Solving the EoMs (S4) to obtain the thermodynamic quantities $(T, \mu_B, B_T, M, S, \chi_B, p_z)$. Verify whether these (T, μ_B, B_T) cover the range of lattice QCD data. If not, adjust (A_h, ϕ_h, B_F). If they do, compare this set with the corresponding lattice data for $(M, S, \chi_B, \Delta p_z)$. If consistent, terminate the process. If not, adjust $\hat{Z}(\phi)$ and repeat the process. Adjustments to $\hat{Z}(\phi)$ are made through gradient descent, where L represents the loss function and ξ are the network parameters used to mimic $\hat{Z}(\phi)$. $\frac{\partial \mathrm{L}}{\partial \xi}$ indicates the direction of descent for the loss function. When the loss function reaches its minimum, it signifies the optimal solution for $\hat{Z}(\phi)$.

where $\dot{\Theta}(z)$ is to take the derivative with respect to the argument and $z = 1/r, z\Phi(z) = \phi(\frac{1}{r}), F(z) = z^2 f(\frac{1}{r}), A(z) = A_t(\frac{1}{r})$, $\hat{Z}'(\Phi)$ is the derivative with respect to Φ. One can refer to the precise definitions of these functions of (S4). Ξ is a five-component vector. Θ contains scalar field ϕ, metric components f, g, η, and Maxwell field A_t. These equations of motion (S18) can be rewritten as a discrete difference equation:

$$\Theta_{i+1} = \Theta_i + \Xi(z_i, \Theta_i, \dot{\Theta}_i(z), \hat{Z}(\Phi_i), \hat{Z}'(\Phi_i), B_F)dz\,, \tag{S19}$$

where we discretize the holographic direction z with a step size dz. The index i corresponds to the i-th layer. The equation gives the recursive relationship between the i-th layer and the $i+1$-th layer. Θ_i corresponds to the field value at the i-th layer. Here, $i = 1$ represents the event horizon, and $i = N$ corresponds to the UV boundary. As shown in Fig. S2, the difference equation can be naturally understood as a $6 \times N$ network without activation function.

Here, we select four thermodynamically independent data sets $\boldsymbol{S}$ that contain quantities $\boldsymbol{S} = \{M, s, \chi_B, \Delta p_z\}$ for an accurate comparison between the holographic model and Lattice QCD data, performing a global fitting. The key problem is to minimize the loss function by optimizing the functional $\hat{Z}(\phi)$. To determine the optimizing direction of $\hat{Z}(\phi)$, one needs back propagation of the neural network to extract the data associated with $\frac{\partial \mathrm{L}}{\partial \xi}$. $\xi \in H$ is any parameters in $\hat{Z}$ neural networks. And, we choose loss function $\mathrm{L} = \mathrm{L}(M, s, \chi_B, \Delta p_z)$ as mean-square error (MSE). Here, we apply a similar definition of the loss function offered by [S9]. The precise form of loss function L is

$$\mathrm{L} = \sum_{I \in \boldsymbol{S}} P_I (I_{\mathrm{LQCD}} - I_{\mathrm{HQCD}})^2\,, \tag{S20}$$

where $I_{\mathrm{LQCD}}, I_{\mathrm{HQCD}}$ correspond to the thermal dynamical quantities $\boldsymbol{S}$ of lattice QCD data and are predicted by

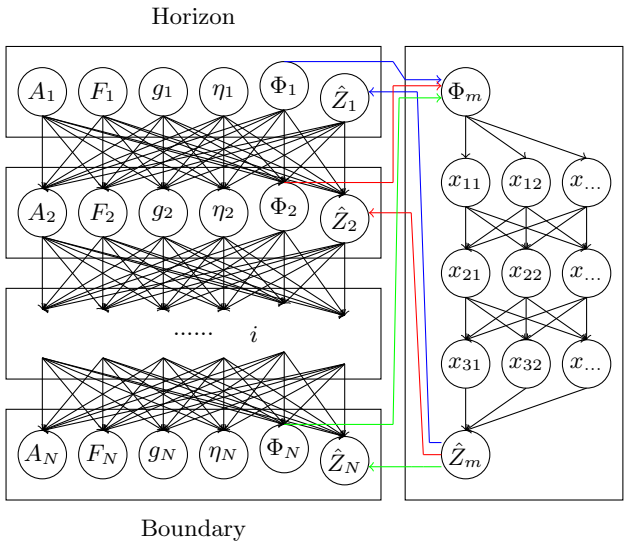

FIG. S2. Discrete network representation of the recursive relationship between layers in solving (S18). Initial conditions are set at the event horizon ($i = 1$), and layers extend to the UV boundary ($i = N$). Each layer i corresponds to field values Θ_i. The network discretizes the holographic direction z into steps dz. $\hat{Z}(\Phi)$ is modeled by a feed-forward network with three hidden layers. $\{x_{11}, x_{12}, \dots\}$ is outputs of the hidden layer. The colored arrows (e.g. green, blue, red) indicate different layers sharing the same functional form of $\hat{Z}(\Phi)$. The arrow is the forward propagation direction, and the arrow opposite is the back propagation direction.

holographic QCD, respectively. The P_I is the inverse of the uncertainty, the maximum difference between the LQCD data and its central value.

We must input $\frac{\partial \mathrm{L}}{\partial \xi}$ and ξ into Adam to minimize the loss function. The key issue is to collect $\frac{\partial \mathrm{L}}{\partial \xi}$. For the i-th layer, we have the following chain rule:

$$\frac{\partial \mathrm{L}}{\partial \xi_i} = \frac{\partial \mathrm{L}}{\partial \Theta_{i+1}} \frac{\partial \Theta_{i+1}}{\partial \xi_i} \,. \tag{S21}$$

Here, ξ_i is the ξ of the i-th layer, Θ_i is the Θ of the i-th layer. One has to note $\xi_i = \xi_j, i \neq j$ that means ξ_i in each layer are the same, but $\frac{\partial \mathrm{L}}{\partial \xi_i} \neq \frac{\partial \mathrm{L}}{\partial \xi_j}$. From (S19), at each layer it can be expressed by

$$\frac{\partial \mathrm{L}}{\partial \xi_i} = \frac{\partial \mathrm{L}}{\partial \Theta_{i+1}} \frac{\partial \Xi(z_i, \Theta_i, \hat{Z}(\Phi_i), \hat{Z}'(\Phi_i), B_F)}{\partial \xi_i} dz \,. \tag{S22}$$

Finally, for the whole network, the key ingredient $\frac{\partial \mathrm{L}}{\partial \xi_i}$ is the sum of all partial derivatives:

$$\frac{d\mathrm{L}}{d\xi} = \int \frac{\partial \mathrm{L}}{\partial \Theta} \frac{\partial \Xi}{\partial \xi} dz = \int \frac{\partial \mathrm{L}}{\partial \Theta} \left(\frac{\partial \Xi}{\partial \hat{Z}} \frac{\partial \hat{Z}}{\partial \xi} + \frac{\partial \Xi}{\partial \hat{Z}'} \frac{\partial \hat{Z}'}{\partial \xi} \right) dz \,.$$

To obtain the first factor of the integrant in (S23), we can make use of the following chain rule for the two neighborhood layers:

$$\frac{\partial \mathrm{L}}{\partial \Theta_i} = \frac{\partial \mathrm{L}}{\partial \Theta_{i+1}} \frac{\partial \Theta_{i+1}}{\partial \Theta_i} \,, \tag{S23}$$

where $\frac{\partial \mathrm{L}}{\partial \Theta_i}$ represents the derivative of each component in Θ at the i-th layer, with the component index omitted for clarity. Here, $\frac{\partial \Theta_{i+1}}{\partial \Theta_i}$ is a 5×5 matrix. From (S19), we obtain:

$$\frac{\partial \mathrm{L}}{\partial \Theta_i} = \frac{\partial \mathrm{L}}{\partial \Theta_{i+1}} \frac{\partial \Theta_{i+1}}{\partial \Theta_i} = \frac{\partial \mathrm{L}}{\partial \Theta_{i+1}} \left(1 + \frac{\partial \Xi(z_i, \Theta_i, \dot{\Theta}_i(z), \hat{Z}(\Phi_i), \hat{Z}'(\Phi_i), B_F)}{\partial \Theta_i} dz \right) . \tag{S24}$$

For convenience, let y_i denote $\frac{\partial \mathrm{L}}{\partial \Theta_i}$, and y denote $\frac{\partial \mathrm{L}}{\partial \Theta}$. Then, the above equation can be written as:

$$y_i = y_{i+1}\left(1 + \frac{\partial \Xi(z_i, \Theta_i, \dot{\Theta}_i, \hat{Z}(\Phi_i), \hat{Z}'(\Phi_i), B_F)}{\partial \Theta_i} dz\right), \tag{S25}$$

which corresponds to the following differential form:

$$y'(z) = -y(z)\frac{\partial \Xi(z, \Theta, \dot{\Theta}(z), \hat{Z}(\Phi), \hat{Z}'(\Phi), B_F)}{\partial \Theta}. \tag{S26}$$

To simplify our notations, we note that this set of equations involves five unknown functions as shown in (S18), and $\frac{\partial \Xi}{\partial \Theta}$ is a 5×5 matrix.

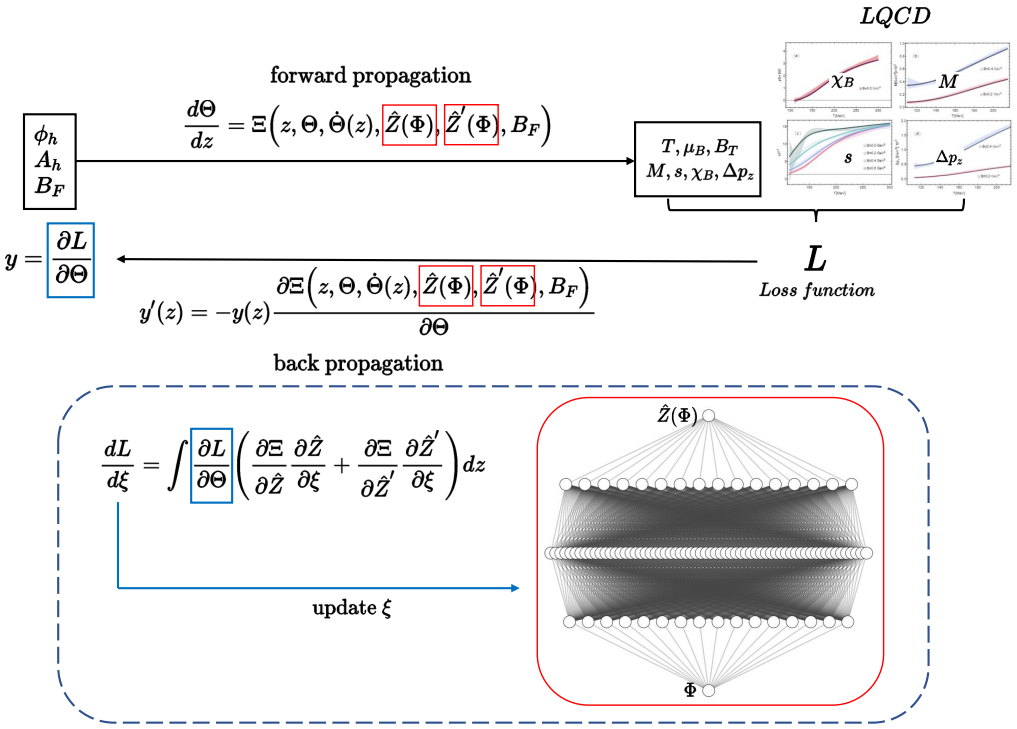

FIG. S3. Continuous representation of our numerical simulation. The top panel depicts the forward propagation, integrating from the infrared (IR, left) to the ultraviolet (UV, right), and comparing with lattice data to compute the loss function. This continuous approach corresponds to Fig. 6. During forward propagation, the function $\hat{Z}$ acts as a numerical component within the equations of motion (EOM). The bottom panel (excluding the dashed section) illustrates back propagation in the continuous limit. By deriving backward integral equations from the forward ones, we calculate the derivative of the loss function L with respect to the parameters ξ, subsequently updating the parameters in the $\hat{Z}(\phi)$ neural network (dashed section). Specifically, $\frac{\partial \hat{Z}}{\partial \xi}$ and $\frac{\partial \hat{Z}'}{\partial \xi}$ are obtained through the internal back propagation of $\hat{Z}$ across the entire integration domain.

We elaborate on the forward and back propagation for the discrete case and derive the continuous form used in practical computations. In the actual calculation, as shown in Fig. S3, we first perform a forward propagation integral to obtain the loss function, and then the derivative of the loss function with respect to the parameters can be propagated through the back differential equation, which used for optimizing the trial function $\hat{Z}(\Phi)$ via gradient descent to minimize the loss function L. The forward and back propagation of the $\hat{Z}$ neural network are respectively regarded as numerical functions participating in the forward and back differential equations.

Finally, we combine all the elements in (S23) and input them into the Adam optimizer to achieve the functional $\hat{Z}(\phi)$, which is a crucial point of this work. We manage to obtain the numerical data for $\hat{Z}(\phi)$ as shown in Fig. S4. It can be good approximated using the following analytical form:

$$\begin{aligned}\hat{Z}(\phi) = {} & a_0 e^{-a_1(\phi - a_2)^2} + a_3 e^{-a_4(\phi - a_5)^2 - a_6(\phi - a_7)^4} \\ & + a_8 \mathrm{sech}[-a_9(\phi - a_{10})^2] + a_{11} e^{-a_{12}(\phi - a_{13})^6} + a_{14}\,,\end{aligned} \tag{S27}$$

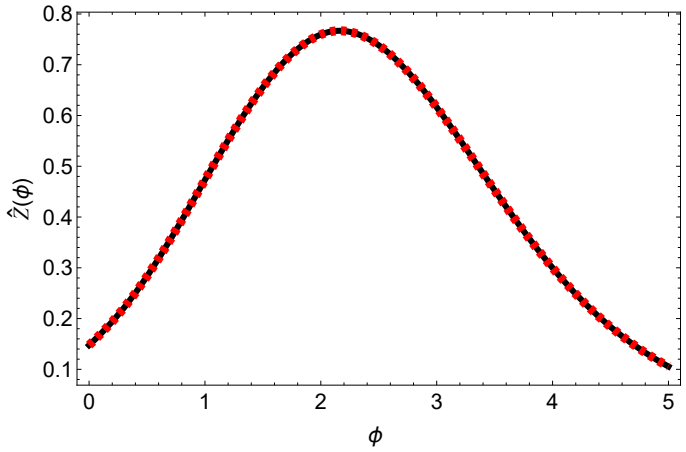

FIG. S4. The magnetic coupling $\hat{Z}(\phi)$ as a function of ϕ. The black solid curve is the one obtained from our neural ODEs architecture. The red dotted curve denotes the one using the analytical function of (S27).

where the parameters are given by

$$
\begin{aligned}
a_0 &= \frac{49677}{100000}, & a_1 &= \frac{8583}{25000}, & a_2 &= \frac{202953}{100000}, \\
a_3 &= \frac{15371}{50000}, & a_4 &= \frac{6297}{50000}, & a_5 &= \frac{39131}{20000}, \\
a_6 &= \frac{411}{50000}, & a_7 &= \frac{413981}{100000}, & a_8 &= \frac{97}{4000}, \\
a_9 &= \frac{34873}{100000}, & a_{10} &= \frac{29503}{50000}, & a_{11} &= -\frac{287}{50000}, \\
a_{12} &= \frac{24319}{12500}, & a_{13} &= \frac{2637}{2500}, & a_{14} &= -\frac{691}{50000}.
\end{aligned}
\tag{S28}
$$

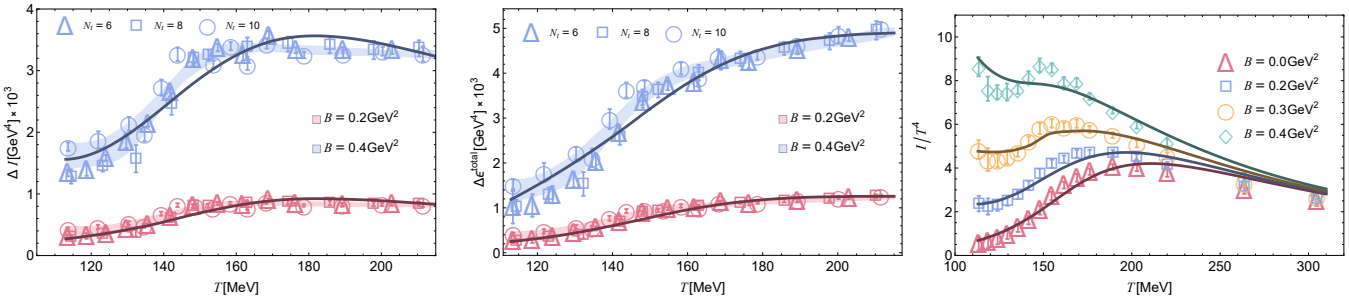

FIG. S5. The renormalized trace anomaly ΔI (left), the renormalized energy density $\Delta\epsilon = \epsilon|_B - \epsilon|_{B=0}$(middle) and the trace anomaly I(right). Our holographic computations (solid curves) are compared with the latest lattice QCD results from [S6]. The N_t corresponds to three lattice spacings, and B denotes the magnetic field strength. The shaded areas correspond to lattice continuum estimates.

To illustrate the efficacy of the algorithm, we present a comparison of four thermodynamically independent quantities, $\boldsymbol{S} = \{M, s, \chi_B, \Delta p_z\}$, between the holographic predictions and the lattice QCD simulations, as shown in Fig.1 of the main text. Additionally, we confirm that the corresponding trace anomaly I, the renormalized longitudinal pressure Δp_z, and the renormalized anomaly ΔI predicted by the holographic model align with the lattice QCD data [S6], as depicted in Fig. S5. This work represents the first quantitative realization of state-of-the-art lattice QCD data [S6] within a holographic model.

[S1] R. G. Cai, S. He, L. Li and Y. X. Wang, "Probing QCD critical point and induced gravitational wave by black hole physics," Phys. Rev. D **106** (2022) no.12, L121902 [arXiv:2201.02004 [hep-th]].

[S2] T. Akutagawa, K. Hashimoto and T. Sumimoto, "Deep Learning and AdS/QCD," Phys. Rev. D **102**, no.2, 026020 (2020) [arXiv:2005.02636 [hep-th]].

[S3] K. Hashimoto, H. Y. Hu and Y. Z. You, "Neural ordinary differential equation and holographic quantum chromodynamics," Mach. Learn. Sci. Tech. **2**, no.3, 035011 (2021) [arXiv:2006.00712 [hep-th]].

[S4] K. Hashimoto, K. Ohashi and T. Sumimoto, "Deriving the dilaton potential in improved holographic QCD from the chiral condensate," PTEP **2023**, no.3, 033B01 (2023) [arXiv:2209.04638 [hep-th]].

[S5] X. Chen and M. Huang, "Machine learning holographic black hole from lattice QCD equation of state," Phys. Rev. D **109** (2024) no.5, L051902 [arXiv:2401.06417 [hep-ph]].

[S6] G. S. Bali, F. Bruckmann, G. Endrődi, S. D. Katz and A. Schäfer, "The QCD equation of state in background magnetic fields," JHEP **08**, 177 (2014) [arXiv:1406.0269 [hep-lat]].

[S7] Kingma, D. P., Ba, J., "Adam: A method for stochastic optimization," [arXiv:1412.6980].

[S8] R. T. Q. Chen, Y. Rubanova, J. Bettencourt, and D. K. Duvenaud, "Neural Ordinary Differential Equations," Advances in Neural Information Processing Systems, vol. 31, 2018.

[S9] S. Shi, L. Wang and K. Zhou, "Rethinking the ill-posedness of the spectral function reconstruction — Why is it fundamentally hard and how Artificial Neural Networks can help," Comput. Phys. Commun. **282**, 108547 (2023) [arXiv:2201.02564 [hep-ph]].